ELSEVIER

Journal of Molecular Catalysis A: Chemical 168 (2001) 209–224

JOURNAL OF MOLECULAR CATALYSIS A: CHEMICAL

www.elsevier.com/locate/molcata

Cobalt-containing catalysts supported by synthetic Zn- and Mg-stevensites and their performance in the Fischer–Tropsch synthesis

Alexander A. Khassin*, Tamara M. Yurieva, Galina N. Kustova, Lyudmila M. Plyasova, Izabella Sh. Itenberg, Margarita P. Demeshkina, Galina K. Chermashentseva, Vladimir F. Anufrienko, Vladimir I. Zaikovskii, Tatyana V. Larina, Irina Yu. Molina, Valentin N. Parmon

Boreskov Institute of Catalysis, 5, Pr. Lavrentieva, Novosibirsk 630090, Russia

Received 21 June 2000; accepted 6 November 2000

Abstract

Co-containing catalysts supported onto the synthetic stevensites of Zn and Mg were prepared using various methods. The evolution of the catalyst structure was monitored during the calcination and a reductive treatment. During the calcination, Co^{2+} cations substitute the divalent cations of the support, that leads to the formation of the mixed Co–Me-stevensite. These Co species cannot be reduced at temperatures below 700°C. The phase composition of the catalyst after the reduction at 500°C contains Co^0 particles supported by the Co–Me mixed stevensites. Unexpectedly, the performance of the Co/stevensite catalysts in the Fischer–Tropsch synthesis was much worse, than that of Co/MgO. The supposition on the metal-support interaction, which causes the low electron-donor capacity of the metallic Co may explain the experimental data.

Keywords: Cobalt; Clays; Silica; Fischer–Tropsch synthesis; Metal-support interaction

1. Introduction

Silica can be considered as a promising support for Co-containing catalysts of the Fischer–Tropsch synthesis (FTS), due to its high specific area and inertness in the FTS conditions.

Numerous studies on Co/SiO_2 as a catalyst for the FTS evidence, that calcined catalysts, prepared at low pH of a maternal aqueous solution, have the phase composition of $Co_3O_4 + SiO_2$, exhibiting no interaction of the metal oxide with the silica support (see, e.g. [1–4]). For these catalysts, the problem of Co^0 sintering during the catalyst reduction is important. The process of Co^0 sintering can be decelerated by activating the catalyst in the flowing hydrogen with a low temperature increment rate ($\sim$0.2 K min^{-1}) [5,6], which is, however, hardly possible in the industrial conditions.

From another side, the Co/SiO_2 catalysts prepared using aqueous solutions at pH $>$ 4, contain up to 100% of cobalt cations loaded in a "hard-reducible" state [3,4,7–11]. In this case, the activity of the reduced

* Corresponding author. Tel.: +7-383-2-344109; fax: +7-383-2-343056.
E-mail address: yurieva@catalysis.nsk.su (A.A. Khassin).

1381-1169/01/$ – see front matter
PII: S1381-1169(00)00530-6

catalysts is low and might be attributed to the "reducible" part of Co only, which have not reacted with the silica support due to a probable inhomogeneity of the preparation. It was reported in [11], that the most of the "hard-reducible" cobalt species, which comprise the calcined Co/SiO_2 catalysts, are very likely the 2:1 trioctahedral layered silicate (stevensite) of Co, namely $Co_3[Si_4O_{10}](OH)_2{\cdot}nH_2O$. At high pH (ca. 12) of the maternal solution used during the catalyst preparation, the formation of (1:1) trioctahedral layered silicate of Co, $Co_3Si_2O_5(OH)_4{\cdot}nH_2O$, was observed in [10].

Being reduced at 800°C, the samples of the Co-stevensite as well as of the Co–Zn-stevensite demonstrated XRD patterns of dispersed Co^0 with diameter of the metallic particles ca. 200–300 Å, as it is determined from XRD [12]. However, these samples were found to be absolutely inactive in the Fischer–Tropsch synthesis. High resolution electron microscopy data (with the resolution of 1.4 Å) on the Co-stevensite reduced at 800°C evidence that the metallic cobalt crystallites are covered with a 20–50 Å film of some amorphous oxide (plausibly, SiO_2). Reoxidation of such samples in the static air does not occur with a significant rate at temperatures below 300°C and has a maximal rate at 530°C (at the temperature increment rate 10 K min^{-1}). This indicates, that the Co^0 particles are not accessible to the molecules of the gaseous phase. Thus, for preparation of active FTS catalysts the formation of unreducible species (i.e. the Co-stevensite as well as an anhydrous Co silicates) have to be avoided, if possible.

An addition of rare-earth metals, Zr and other metals as promoters to the Co/SiO_2 catalysts was studied in many papers [13–17] and had been found to be an effective way to decreasing the temperature of the Co^{2+} reduction. Probably the promotion of Co/SiO_2 helps to prevent the formation of Co-stevensite. However, even the promoted Co-containing catalysts do not exhibit 100% reducibility of the Co cations: it is reported to be about 95% for the Zr-promoted Co/SiO_2 [16], and to be less than 50% for the La^{3+} promoted Co/SiO_2 [13].

Here, we present studies on the Co-containing catalysts, supported by the synthetic stevensite of Zn ($Zn_3[Si_4O_{10}](OH)_2{\cdot}nH_2O$) and that of Mg ($Mg_3[Si_4O_{10}](OH)_2{\cdot}nH_2O$). We hoped, that this would give us a chance to stabilize a joint Co–Me oxide (Co–Zn spinel or solid solution of Zn^{2+} in the anion-modified CoO or a Co–Mg mixed oxide) in the porous structure of the stevensite support. By taking into the consideration, that the Zn-stevensite (zincsilite) has been shown previously [18] to have a very perspective morphology for serving as a good support and is stable at least up to 500°C, it could be considered as a good opportunity for the creation of an effective catalyst of the Fischer–Tropsch synthesis. Below we present the results of our investigation of the Co-containing catalysts supported by synthetic stevensites of Mg and Zn and considering their structural evolution during their activation as well as their catalytic properties in the FTS.

2. Experimental section

2.1. Preparation of the catalysts

The synthetic stevensite supports were prepared by a homogeneous deposition-precipitation method using the urea decomposition for the pH control [19] as it was reported in [11]. The obtained supports are hereinafter denoted 'zincsilite' or ZS ($Zn_3[Si_4O_{10}](OH)_2{\cdot}nH_2O$), and 'stevensite' or MS ($Mg_3[Si_4O_{10}](OH)_2{\cdot}nH_2O$).

Five Co-containing catalysts were prepared. Three Co–Zn–ZS catalysts were prepared by stoichiometry Co:Zn:ZS = 5:1:2. Two Co–Mg–MS catalysts were prepared by stoichiometry Co:Mg:MS = 5:1:2.

The catalysts prepared by co-precipitation technique are further denoted as P/ZS and P/MS. The precipitation was performed from a stoichiometric 10 wt.% aqueous solution of the corresponding nitrates ('pure for chemical analysis' grade, Uralian plant of chemicals, Russia) at 60–70°C. A mixture of water solutions of NaOH and Na_2CO_3 was used as the precipitants. pH of the precipitation was 7.0 for the P/ZS and 10.5 for the P/MS catalysts. The synthetic stevensite support was slurried in the maternal solution before starting the catalyst preparation. Catalysts P/ZS and P/MS were washed thoroughly by distilled water and dried overnight by an IR lamp in air.

The catalysts prepared by the incipient wetness impregnation technique from the corresponding nitrates and acetates are further denoted as N/ZS, A/ZS and A/MS. An amount of 10 wt.% aqueous solutions of

the salts were used. The catalysts were dried overnight by an IR lamp in air.

2.2. Characterization techniques

In situ thermal gravimetry (STA) data were obtained by means of a Netzsch STA 409 thermal balance. The sensitivity of weight determining was about 0.1 mg (ca. 0.1% of the sample weight). Heating rate was $10\,K\,min^{-1}$ at measurements in argon flow and in air, and it was $5\,K\,min^{-1}$ at measurements in hydrogen flow. Parameters for the STA TPR studies were optimized in order to minimize criterion P defined in [20,21]: $P = \beta S_0/FC_0$, where β is the heating rate ($K\,min^{-1}$); F the flow rate ($ml\,min^{-1}$); C_0 the initial H_2 concentration ($mol\,ml^{-1}$); S_0 the amount of reducible species in the sample (mol). The value of P should be at least lower than 20 K. In our studies $P \approx 5(5 \times 10^{-4})/150/(4.5 \times 10^{-5}) \approx 1.7\,K$.

The accuracy of determining Co reduction degree by means of temperature programmed reduction and temperature programmed oxidation STA measurements may be estimated as ca. 10%.

X-ray diffraction (XRD) studies were done with Siemens D-500 diffractometer using the Cu Kα radiation. Ex situ XRD measurements of calcined and reduced samples were done in air soon after samples exposure to air. In situ measurements were held in a homemade chamber described elsewhere [22].

Infrared transmission spectra (IRS) were recorded in a range of 300–4000 cm^{-1} by FTIR spectrometer Bomem MB-102. Powdered catalyst samples were diluted with CsI (or KBr), or the catalyst powder emulsions were prepared using a fluorinated oil.

Diffusive reflectance spectra (DRS-UV–VIS) were recorded in the range 11,000–50,000 cm^{-1} by a Shimadzu 2501PC UV spectrometer.

The electron microscopy (TEM and HREM) data were obtained by electron microscopes JEM-100CX (JEOL, Japan) with a 4.5 Å resolution and JEM-2010 with a 1.4 Å resolution. The samples for the electron microscopy were prepared by making an ethanol suspension, its dispersing by ultrasound and deposing onto an undercoat of a "holey" carbon films.

For calcination and reduction we used 99.99% purity Ar and 99.9% purity H_2, which were additionally purified from O_2 traces to 0.1 ppm over a Ni–Cr catalyst, and also from water by silica gel.

2.3. Catalytic tests

Catalytic tests were held in a slurry reactor under atmospheric pressure ($P = 1.2$–1.3 atm), and H_2:CO ratio at reactor inlet was 2. *N*-tetradecane, *n*-$C_{14}H_{30}$, was used as a filling. Slurry temperature was varied from 463 to 503 K with an accuracy of ±1 K. Inlet gas also contained 10% of N_2 used as internal standard.

Slurry volume was 20 cm^3, and catalyst sample weight varied from 1 to 2 g. Catalyst powder with particles less than 0.18 mm was used for the purpose. Inlet gas velocity was varied from 0.3 to $1.2\,l\,h^{-1}$, which seemed to have no influence on the catalyst activity or selectivity. Gas feed was organized under a single bubble regime, average bubble diameter being ca. 0.2 mm, and residence time being ca. 3 s. The mass transfer coefficients of reactants in the slurry could be estimated by the Mu–Yang model [23] as 0.03–0.04 $cm\,s^{-1}$, so the value of ($k_L a$) was 50 times higher, than the observed rates of CO conversion. This fact evidences that reactant diffusion is not the rate limiting stage. Here a is the area of gas bubbles, which are resident in the slurry at a given moment.

Products were analyzed regarding gaseous products (C_1–C_8), condensate (C_8–C_{15}) and hydrocarbon fraction C_{11+} dissolved in the slurry. These products were analyzed with TSVET-530 (USSR) chromatograph equipped by a column packed with γ-Al_2O_3 (fraction C_1–C_8) and with TSVET-560 (USSR) chromatograph equipped by a glass capillary with phase SE-30 (for the C_{8+} fractions). As proved by special tests, the values of the Anderson–Schultz–Flory (ASF) parameter α, calculated from the C_2–C_8 fraction and from the C_{15+} fraction (dissolved in the slurry), differed by less than 0.02, which is close to the measurements accuracy. So, α-value was usually calculated solely from the data on fraction C_2–C_8.

The relative accuracy of methane formation rate in a single measurement was ±18%. With five measurements it was possible to achieve an accuracy of ±11%. The relative accuracy of CO conversion rate determining was rather poor and equaled ±25%. This accuracy could be improved to ±20% by making several measurements. When determining the ASF parameter α, accuracy was much better, since not the absolute values, but only the ratio of C_{n+1} and C_n formation rates was important. Thus, the accuracy of α-value determining was ±0.015.

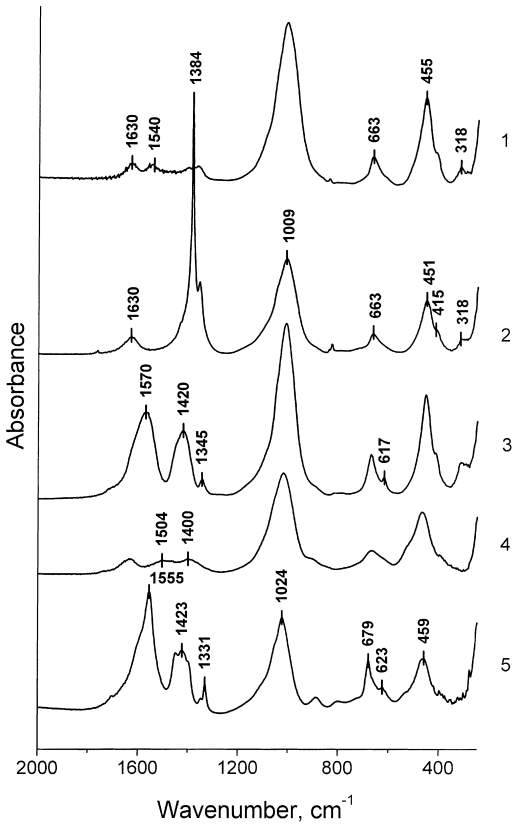

Fig. 1. IR spectra of the uncalcined samples under study: (1) P/ZS; (2) N/ZS; (3) A/ZS; (4) P/MS; (5) A/MS.

3. Results and discussion

3.1. Characterization of the catalysts

3.1.1. Uncalcined catalysts

The IR spectra of the uncalcined samples were measured to determine their phase composition (see Fig. 1). A stevensite-type layered silicate (which was used as a support and exhibits absorption at ca. 460, 660 and 1010 cm^{-1} [11]) and either Co^{2+} hydroxycarbonate (absorption at 1300–1500 cm^{-1}), or nitrate (absorption at ca. 1384 cm^{-1}) or acetate (absorption at ca. 615–620, 1345, 1420 and 1570 cm^{-1}) species (depending on the nature of the cobalt cations source) were found to comprise the uncalcined samples. Data of [24] were used for the band attributions.

Recently, we have shown [11] that the cationic composition of stevensites affects the position of the ν(OH) absorption band, as well as the temperature of decomposition of the stevensite structure, followed by an anhydrous silicate crystallization. For the case, the positions of the ν(OH) vibration absorption bands were found to be equal to those of the pure stevensite and zincsilite. Indeed, they were found to have the maximal absorbancy at 3639 cm^{-1} for the case of the Co/ZS catalysts and at 3678 cm^{-1} for the case of those supported by Mg-stevensite. Thus, it indicates no significant interaction of Co^{2+} with the support (at least less than 20% of the present Co) at the stage of the catalyst preparation.

3.1.2. Calcination of the catalysts

The calcination of the catalysts in the inert gas flow is accompanied by a decomposition of the Co salts. The experimental STA profiles are given in Fig. 2. These profiles are close to the superposition of those reported earlier for pure $Co(NO_3)_2 \cdot 6H_2O$ [1] (or Co acetate (according to our data) or Co hydroxycarbonate [25]) and the stevensite support [11]. An important difference of the experimental profiles from the superposition of the profiles of the corresponding pure substances is a lower temperature of an exothermic effect in the range 700–900°C, which was earlier attributed to the crystallization of anhydrous silicate being attendant to decomposition of the layered silicate [11].

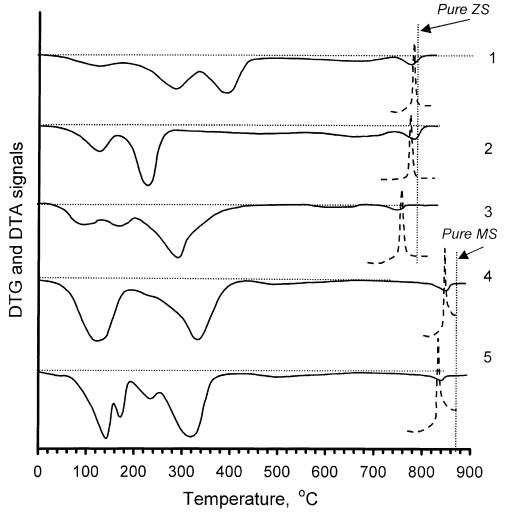

Fig. 2. STA data (DTG: solid line; DTA: dashed line) on the calcination of the samples: (1) P/ZS; (2) N/ZS; (3) A/ZS; (4) P/MS; (5) A/MS.

$$Zn_3Si_4O_{10}(OH)_2 \cdot n(H_2O) \overset{790^\circ C,\text{exothermic}}{\rightarrow} \tfrac{3}{2}Zn_2SiO_4 + \tfrac{5}{2}SiO_2 + (n+1)H_2O$$

$$Mg_3Si_4O_{10}(OH)_2 \cdot n(H_2O) \overset{870^\circ C,\text{exothermic}}{\rightarrow} \tfrac{3}{2} \times (MgSiO_3 + MgO) + \tfrac{5}{2}SiO_2 + (n+1)H_2O$$

$$(Co_{1/2+x}, Me_{1/2-x})_3Si_4O_{10}(OH)_2 \cdot n(H_2O) \overset{\text{above } 710^\circ C,\text{exothermic}}{\rightarrow} 3\left\{\left(\tfrac{1}{2}-x\right)MeSiO_3 + xCoSiO_3 + \tfrac{1}{2}CoO\right\} + \tfrac{5}{2}SiO_2 + (n+1)H_2O$$

$$(Co_{1/2-x}, Me_{1/2+x})_3Si_4O_{10}(OH)_2 \cdot n(H_2O) \overset{\text{above } 710^\circ C,\text{exothermic}}{\rightarrow} 3\left\{\tfrac{1}{2}MeSiO_3 + xMeO + \left(\tfrac{1}{2}-x\right)CoO\right\} + \tfrac{5}{2}SiO_2 + (n+1)H_2O$$

In [11], we also reported, that the temperature of exothermic crystallization of the anhydrous silicate depends on the cationic composition of initial stevensite. The crystallization occurs at 870°C for the Mg-stevensite, at 790°C for the Zn-stevensite, at 710°C for the Co-stevensite. For the mixed Co–Zn-stevensites, the temperature of the crystallization has an intermediate value. Thus, the position of the exothermic crystallization could be used for estimating the amount of Co^{2+}, incorporated in the structure of a stevensite support during the calcination of a catalyst. Table 1 presents the experimental temperatures of the silicate crystallization, T_{cryst}, and amount of Co^{2+}, $Co^{stevensite}$, which interacted with a support (in respect to total Co loading). A linear dependence of T_{cryst} versus the atomic fraction of Co^{2+} in the stevensite composition is assumed in accordance to the data of [11]. Of course, this can be considered as only a rough estimation, but not as a qualitative technique, since no special calibration measurements were made.

The stevensite support composition derived from the STA data for the samples calcined in static air was found to be coincident to those for the samples, calcined in the inert gas flow. Moreover, the STA profiles of the catalyst calcination in the static air up to 500°C were found to be very similar to those for the calcination performed in the flowing inert gas. However, the phase composition was found to depend sufficiently on the conditions of the catalyst treatment, as well as on the nature of the Co^{2+} source (see Table 2). The phase attribution was made mainly according to the XRD patterns and the IR spectra of the calcined samples. The calcination of the samples leads to vanishing the IR absorption in the range of 1300–1500 cm^{-1} (the $CO_3{}^{2-}$-group) for P-samples, 1384 cm^{-1} (the $NO_3{}^-$-group) for the N/ZS sample and 615–620, 1345, 1420, and 1550–1570 cm^{-1} (the CH_3COO^--group) for the A-samples, indicating a decomposition of the initial Co^{2+} species.

Simultaneously, for all Co/ZS samples treated in the static air (as well as for N/ZS sample calcined in the inert gas flow), the absorption band at ca. 575 cm^{-1} and a shoulder at ca. 500 cm^{-1} appear, the intensity of the band at ca. 660 cm^{-1} increases, which might be attributed to the formation of either Co_3O_4 or a Zn–Co spinel phase (see Fig. 3). Actually, the presence of a phase with the spinel-type structure in these samples was detected by XRD. The normal Co_3O_4 is characterized by absorption at 669, 566 and 389 cm^{-1}. The overlap of these bands and those of zincsilite (or Mg-stevensite) does not allow us to analyze the band positions. However, one may conclude, that the vibration at 566 cm^{-1} is apparently shifted to the range of higher energies. Taking into consideration our previous results [26,27], the formation

Table 1
The experimental data on the temperature of the anhydrous silicate crystallization and the estimated data on the amount of Co^{2+} involved to the stevensite structure during the catalysts calcination (see the text)[a]

Sample	P/ZS	N/ZS	A/ZS	P/MS	A/MS
Temperature of anhydrous silicate crystallization T_{cryst} (°C)	775 (761)	773 (770)	755 (747)	847 (803)	833 (786)
Co:Me-stevensite composition	0.22 (0.54)	0.26 (0.31)	0.73 (1.08)	0.16 (0.70)	0.29 (1.06)
$Co^{stevensite}$ fraction (at.%)	22 (41)	25 (29)	51 (62)	17 (49)	27 (62)

[a] The figures in brackets correspond to the samples after the calcination–reduction–oxidation procedure and will be discussed later on.

Table 2
The phase composition of the samples after their calcination in air or in the inert gas flow at 400°C

Sample	Co^{2+} in the stevensite support(%)[a]	CoO and/or MgO[b]	(Co, Zn)Co_2O_4 and/or spinel-type Co_2SiO_4[b,c]	ZnO[b,c]	Color after the calcination at 800°C
Calcination in the flowing inert gas					
P/ZS	22	++	Traces	+	Blue
N/ZS	25	n/d	++	−	Blue
A/ZS	51	++	Traces	+	Blue
P/MS	17	++	+	−	Dark brown
A/MS	27	++	+	−	Dark brown
Calcination in the static air					
P/ZS	22	n/d	++	−	Blue
N/ZS	25	n/d	++	−	Blue
A/ZS	51	+	+	++	Blue
P/MS	17	Traces	++	−	Dark brown
A/MS	27	Traces	++	−	Dark brown

[a] According to temperature of the anhydrous silicate crystallization (STA).
[b] According to XRD data.
[c] According to IRS data.

of mixed oxide $Co_{1-x}Zn_xCo_2O_4$ could be expected for a pure Co–Zn system. It is important to note, that the possibility of the formation of spinel-type Co_2SiO_4 (Co^{2+} in the octahedral positions and Si^{4+} in tetrahedral positions) should not be overlooked (see [3,17]). It is uneasy to discriminate this phase from Co_3O_4, due to close values of the lattice parameter a ($a = 8.08$ Å for Co_3O_4 and 8.14 Å for Co_2SiO_4). The experimental value of the lattice parameter a was found to be close to 8.09 Å for the samples under the study. Thus, at least the formation of a Td(Co^{2+}, Zn^{2+})$_{1-x}$Oh(Co^{2+})$_{2x}$Oh(Co^{3+})$_{2-2x}$Td(Si^{4+})$_x$O$_4$ mixed oxide might be plausible [3]. It is important to note that for all the samples calcined at 450°C, the position of the ν(OH) absorption band of the stevensite support moved slightly to the region of a lower wavenumber (e.g. from 3640 to 3635 cm^{-1} for A/ZS), which is in the agreement with the above conclusion on a partial (up to ca. 50%) substitution of Co^{2+} for Zn^{2+} (or Mg^{2+}) of the stevensite support. The XRD patterns of this sample and the sample P/ZS contain peaks at $2\theta = 47.2$ and 56.6°, which are assigned to ZnO [28].

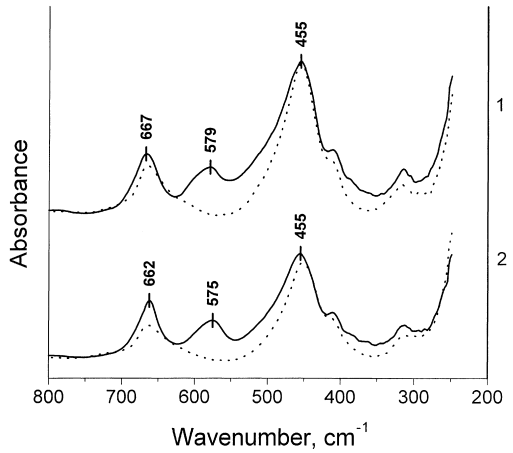

Fig. 3. IR spectra of: (1) the P/ZS sample calcined in air at 450°C; (2) the N/ZS sample calcined in the inert gas flow at 450°C (solid lines) in comparison with the IR spectra of the corresponding uncalcined samples (dotted lines).

According to XRD, during the calcination in the Ar flow, the P/ZS and A/ZS samples transformed mostly into independent CoO and ZnO phases (which can, probably, be solid solutions of Zn^{2+} in an anion-modified CoO and of Co^{2+} in an anion-modified ZnO, correspondingly). However, the discussed above spinel phase is also present in these samples in a trace amount. The IR spectra of the discussed samples do not contain the absorption band at ca. 570 cm^{-1}.

The phase composition of the sample N/ZS after the calcination in the flowing inert gas (Ar) did not exhibited any difference from that after the calcination in static air: the Zn–Co spinel and zincsilite were the only two phases, comprising the samples.

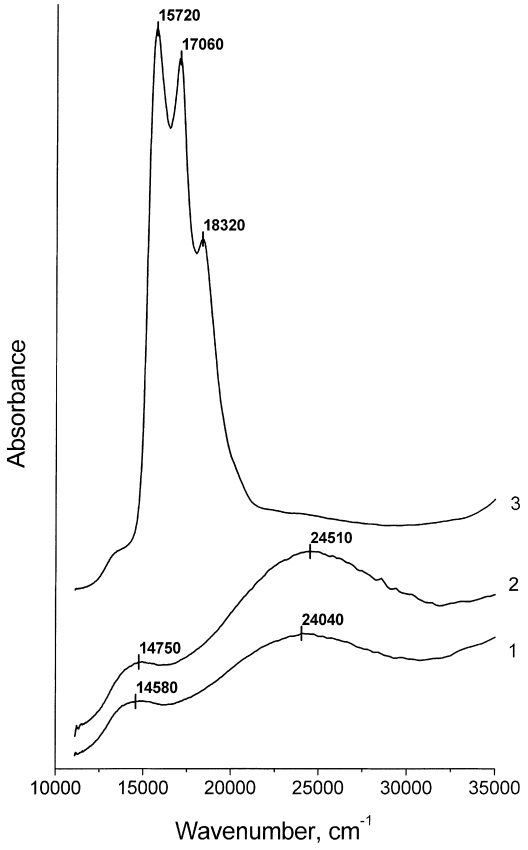

Fig. 4. The DRS UV–VIS spectra of: (1) the P/ZS sample calcined in air at 450°C; (2) the N/ZS sample calcined in air at 450°C; (3) the N/ZS sample calcined in air at 800°C for 12 h.

DRS spectra of sample P/ZS calcined in the static air at 450°C as well as that of similarly treated N/ZS are present in Fig. 4 (curves 1 and 2). An intensive oxide absorption background (due to a Me–O–Me interaction) is registered in the UV–VIS range for these samples. This indicates the probable presence of a Co oxide phase in both P/ZS and N/ZS samples calcined at 450°C. In addition, these spectra exhibit the presence of two wide bands at ca. 14,600 and 24,000 cm^{-1}. It is natural to assume that the observed absorption bands are related to the low-spin state of the Co^{3+} cations in the octahedral oxygenic coordination. In fact, for this case the ground state of the Co^{3+} cations (d^6) is $^1A_{1g}$ and two electron transitions can be observed: $^1A_{1g} \rightarrow {}^1T_{1g}$ and $^1A_{1g} \rightarrow {}^1T_{2g}$. At that the position of the band maxima of Co^{3+} are expected to be shifted in the range of higher energies relatively to the well studied Fe^{2+}, since the extent of the cation oxidation is more high. Thus, we attribute the band at ca. 14,600 cm^{-1} to the transition $^1A_{1g} \rightarrow {}^1T_{1g}$, and the band at ca. 24,000 cm^{-1} to the transition $^1A_{1g} \rightarrow {}^1T_{2g}$ of the low-spin state of the Co^{3+} cations in the octahedral oxygenic coordination. The stabilization of the high-spin state of the Co^{3+} cations (d^6) in the octahedral oxygenic coordination seems to be less probable: if the ground state is $^5T_{2g}$ and the only allowed state is ^5E_g, then the electron transitions can be observed in the range of 10,000–14,000 cm^{-1} only [29].

Thus, a certain Co oxide, which contains Co^{3+} in the octahedral coordination, is present in the samples under discussion. This could be either Co_3O_4 or Zn–Co spinel. The simultaneous presence of CoO also cannot be denied on account of the DRS data.

The color of the Co/ZS samples after the calcination at 800–900°C is blue to “shining” blue. The DRS studies (see Fig. 4, curve 3) revealed an intensive triplet band in the ranges of ca. 15,700, 17,100, 18,300 cm^{-1} which may be attributed to Co^{2+} in a tetrahedral coordination. For a tetrahedrally coordinated Co^{2+} (d^7) cation, the ground state is $^4A_2(e^4t_2^3)$ which excludes the existence of transitions to low-spin excited states. Three quartet-to-quartet transitions are possible: $^4A_2 \rightarrow {}^4T_2(\nu_1)$, $^4A_2 \rightarrow {}^4T_1(F)(\nu_2)$, and $^4A_2 \rightarrow {}^4T_1(P)(\nu_3)$. Literature data (see, e.g. [30]) evidence that in the oxygenic surrounding the bands ν_1 and ν_2 have maxima in the IR range, while the band ν_3 is usually detected in the range 15,000–19,000 cm^{-1}. Triplet splitting of the band ν_3 is related to a distortion of the tetrahedral coordination CoX_4, which gives, most plausibly, the CoX_3Y coordination. The covalence of Co–Y bond is plausible.

The XRD patterns and the IR-spectra of these samples show the existence of SiO_2, Zn_2SiO_4 (Willemite) and a little amount of ZnO. No spinel phase, which could contain Co^{2+} in the tetrahedral coordination, was observed by the IR and XRD techniques. Thus, one should suggest that at the stage of the zincsilite decomposition, some of the Co^{2+} cations are either incorporated into the willemite structure or included into the tetrahedral interstitions of the ZnO structure. In both cases the trigonal distortion of the tetrahedral coordination could take place. No more than 16% at. of Co^{2+} can be dissolved in an ideal ZnO [31], and we failed to find literature data on the dissolution of Co^{2+}

in willemite. However, even small amounts of Co^{2+} in the tetrahedral coordination can cause an intensive absorption. In fact, the extinction coefficient of Co^{2+} in the tetrahedral coordination should be very high, since no center of inversion is present for these species. For example, the sample 0.17 wt.% Co^{2+}/ZnO has the value of the extinction coefficient ca. 120 cm^{-1} at the frequency 15,400 cm^{-1} [30]. Thus, we are hesitant to interpret undoubtedly the nature of these species.

3.1.3. Reduction of the catalysts

The experimental STA TPR profiles of the samples calcined at 450°C are shown in Fig. 5. One can obviously segregate two main regions of weight loss by the samples: in the range of 200–300 and 350–500°C.

The experimental XRD patterns of the reduced at 500°C samples contain both the lines which are attributed to the β-Co^0 phase (the face centered cubic one, [32]) and those attributed to the α-Co^0 phase (the hexagonal one, [33]). However, these patterns cannot be attributed to a mixture of α-Co^0 and β-Co^0 [34]. The width of the lines common to α-Co^0 and β-Co^0 ($(0\,0\,2)_{hex}$ and $(1\,1\,1)_{fcc}$; $(1\,1\,0)_{hex}$ and $(2\,2\,0)_{fcc}$) is about three times less than that of the lines, which are characteristic to any one of the Co^0 modifications

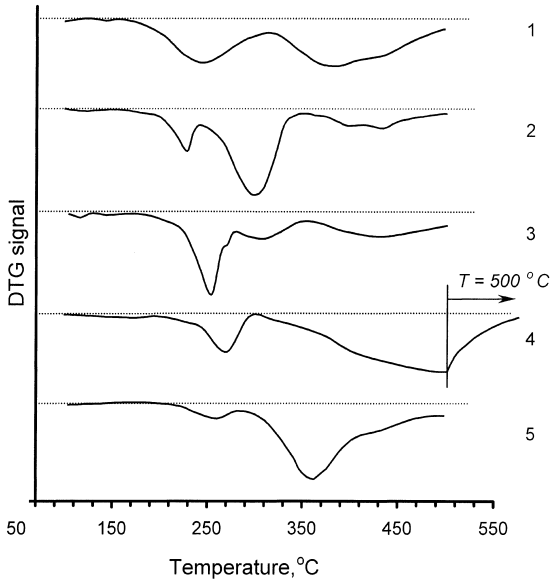

Fig. 5. STA data on the reduction in the hydrogen flow of the samples calcined in the flowing inert gas: (1) P/ZS; (2) N/ZS; (3) A/ZS; (4) P/MS; (3) A/MS.

($(1\,0\,1)_{hex}$ and $(2\,0\,0)_{fcc}$). As it was noted by Wilson [35] and Guinier [36], such distortions of the XRD patterns of Co^0 can be induced by stretched defects of its structure, particularly the interchange of domains with an 'ABCABC' order of the $[1\,1\,1]_{fcc}$ atomic layers (the fcc structure) and domains with an 'ABABAB' order of the same atomic layers (the hex structure). Recently, we observed the formation of such Co^0 particles during carbonization of β-Co^0/MgO in a CO flow [25]. Their structure was proved by a comparison of the experimental XRD patterns with the computer simulated ones [34] and described as a 'defective spacial-modulated interchange of coherent domains with fcc and hex structures'.

Normally, the Co_3O_4 spinel phase reduces in one step at ca. 280°C giving Co^0 or in two steps in temperature ranges of 250 and 350°C giving CoO and Co^0, correspondingly. Despite several explanations were given for this variability of experimental data, its real nature is still unclear. We observed recently [27], that the inclusion of Zn into the structure of the Co_3O_4 oxide shifts the temperature of the Co^{3+} reduction to the region of lower temperatures (240°C was observed for Co:Zn = 5:1 and 190°C for Co:Zn = 2:1). It was shown in the same work, that the temperature of the reduction of the mixed (Co, Zn)O oxide is shifted conversely to the region of higher temperatures (430°C was observed for Co:Zn = 5:1). A similar effect of the CoO promotion with Mg^{2+} was observed in [25].

Here, we incline to attribute the weight loss at 200–300°C to the reduction of a Co(Zn)Co_2O_4 oxide. The weight loss at 350–500°C then should be attributed to the reduction of Co(Zn)O and Co(Mg)O. The incorporation of Si^{4+} cations into the Co oxide structure should also be considered as a factor, which may increase the reduction temperature (see above).

From the termogravymetric data on the catalyst reduction one can estimate the amount of the Co cations comprising the (Zn-)Co_3O_4 and (Zn-, Mg-)CoO phases. The sum of so estimated values and the amount of Co^{2+} in the stevensite support was found to exceed 100% by the factor of 1.1–1.2. Three possible sources of the mistake can be supposed at making the estimations. (1) Deflating of the stevensite support (i.e. the process of water removal from the stevensite interlayer) is apparently goes on during the reduction in the temperature range of above 400–500°C, since the samples were calcined at 450°C. (2) The amount

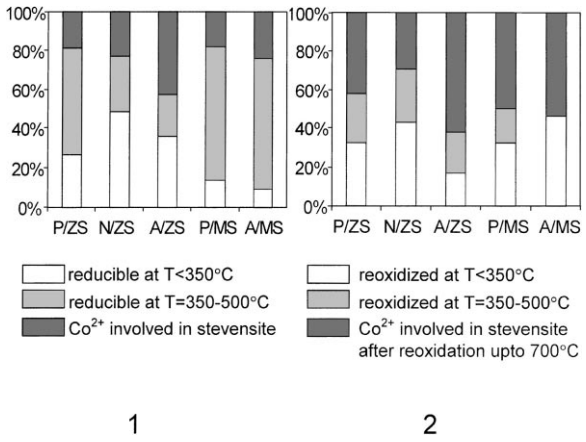

Fig. 6. Histograms of: (1) the Co species distribution in the calcined samples (based on the data of TPR); and (2) the Co species distribution in the reduced samples (based on the data of TP-oxidation) (see the text for details).

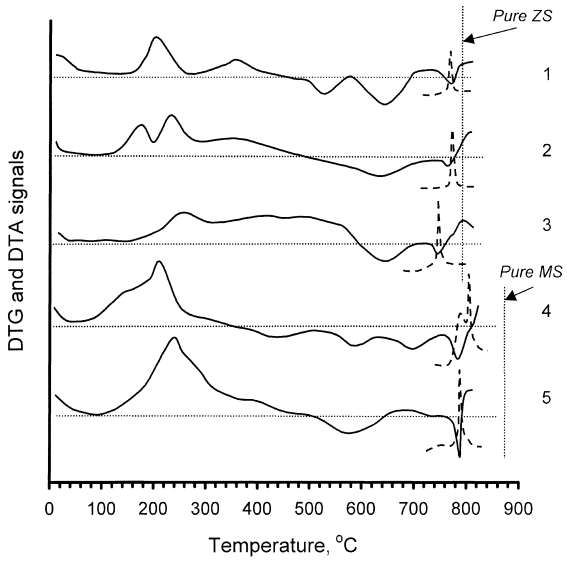

Fig. 7. STA data (DTG: solid line; DTA: dashed line) on the reoxidation of the reduced samples: (1) P/ZS; (2) N/ZS; (3) A/ZS; (4) P/MS; (5) A/MS.

of Co^{2+} in the stevensite support is, probably, overestimated due to the above mentioned roughness of the estimation of the stevensite cationic composition. (3) The gross weight loss includes the removal of anionic admixtures (CO_3^{2-} and/or OH^-) from the oxide structure. Since we cannot make a proper correction of the estimation, we pretend to normalize the total Co amount to 100%, postulating only a 10–20% accuracy of the estimated sample compositions. The resulting distributions of the Co species in the calcined samples are present at graph 1 of Fig. 6.

For clarification of the reduction extent of Co for the reduced samples, we performed the temperature-programmed oxidation studies of the samples reduced at 500°C.

3.1.4. Reoxidation of the catalysts

STA profiles of the reoxidation of the reduced at 500°C samples are shown in Fig. 7.

The reoxidation was performed in the static air medium. The effects of the weight gain at the temperature range less than 400°C are followed by the effects of the weight loss at higher temperatures. The latter are obviously due to further deflating of the stevensite support. The gross weight loss in the range of temperatures 400–700°C was found to be significantly less than it could be expected from the STA data on the treatment of the uncalcined samples in the static air. At the same time, the gross weight gain in the range of temperatures lower than 400°C is much less, than it could be expected for the oxidation of Co^0 to Co_3O_4. The most probable explanation of these data is that some of the Co^0 species are oxidized in the temperature range of above 400°C (see, for example, the reoxidation profile for sample A/ZS (curve 3 in Fig. 7)). It should be noted that, normally, pure Co^0 is oxidized at temperatures below 350°C.

The most reasonable explanation for the observed elevation of the oxidation temperature is a probable encapsulation of Co^0 particles in the pores of the support. Naturally, this would demand the gas O_2 to penetrate through a barrier of a support phase, which would decrease the rate of the oxidation in the medium temperature range.

The temperature of the exothermic Zn (or Mg) anhydrous silicate crystallization was found to move further to the lower temperatures, indicating that after the reoxidation Co^{2+} is incorporated in the stevensite support in more extent, than after the calcination of the samples.

We are not able to estimate properly the amount of Co^0, which oxidizes at the elevated temperatures. We suppose, that the “easy oxidized” Co species do not

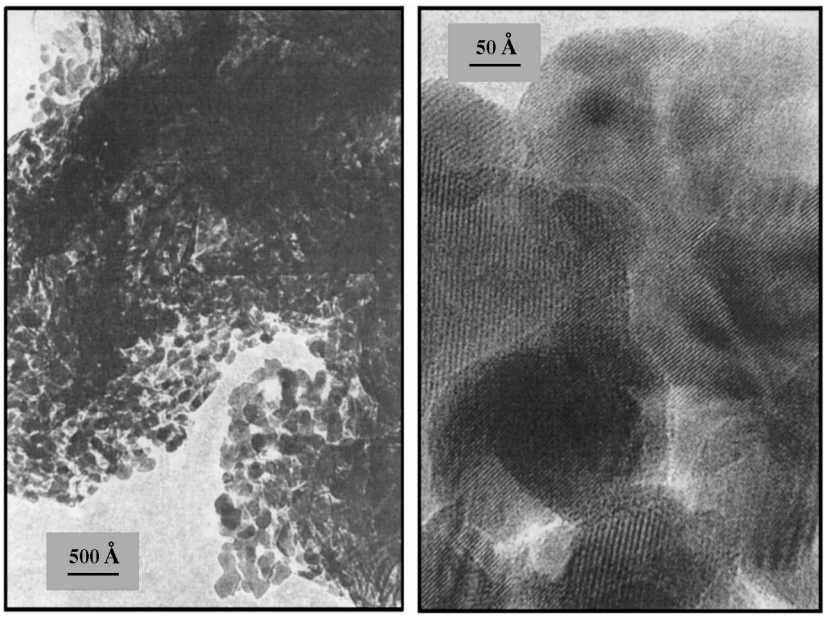

Fig. 8. TEM (left) and HREM (right) images of the sample P/ZS after its treatment in the inert gas flow at 450°C.

interact with the support, while all the "new" stevensite Co^{2+} species are those, which were oxidized at high temperatures. Then the resulting balances of the Co species in the reduced samples will look like it is shown in Fig. 6, graph 2.

Thus, the results of the temperature-programmed oxidation makes it possible to estimate the amount of "easily oxidized" Co^0 species. We suppose, that only these species are active in the Fischer–Tropsch synthesis, since "hardly oxidized" species are, most likely, not available for the molecules of the reactants.

3.1.5. TEM and HREM data on the evolution of P/ZS sample

We would like to illustrate the above described evolution of the samples under the study by the electron microscopy images of the sample P/ZS. Figs. 8–12 present the TEM and HREM images of sample P/ZS during its reduction–oxidation–reduction treatment. Some important observations are noted below.

The TEM and HREM data on the sample P/ZS calcined at 450 in Ar (Fig. 8) evidence that: zincsilite has a very good texture for being an excellent catalyst support. It has morphology of curved plates with the thickness of 50–100 Å; CoO particles with the main size of crystallites ca. 100–400 Å fill the space between the plates of zincsilite.

The TEM data on the sample P/ZS calcined at 450 in Ar and reduced at 450°C (Fig. 9) evidence that:

1. Despite the XRD data discussed above indicate the presence of the defective Co^0 phase, only few

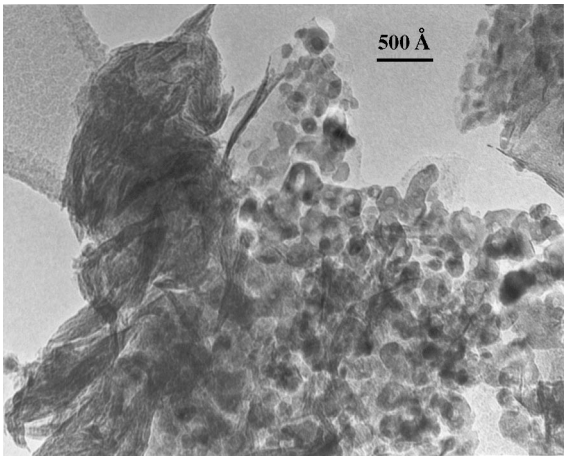

Fig. 9. TEM image of the sample P/ZS after its treatment in the inert gas flow at 450°C and, consequently, in the hydrogen flow at 450°C.

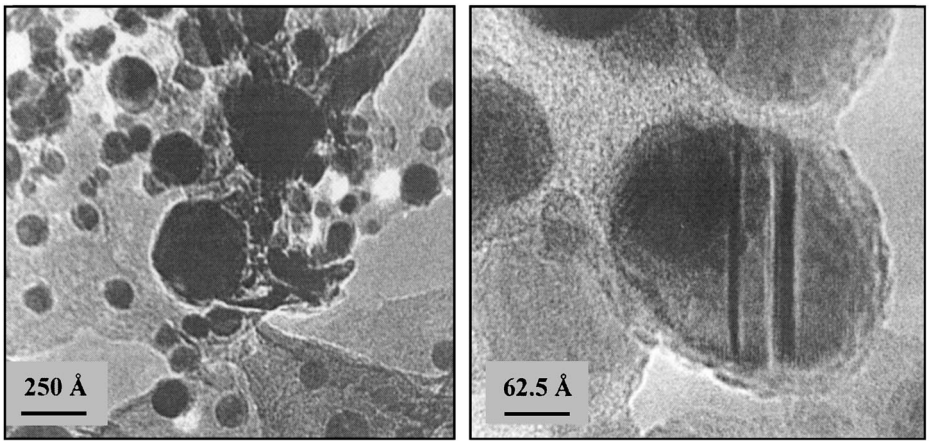

Fig. 10. TEM (left) and HREM (right) images of the sample P/ZS after its consecutive treatment in the inert gas flow at 450°C and the H_2 flow at 800°C.

80–100 Å particles, which may be attributed to Co^0 phase are detected; these particles are covered by thick layer of an amorphous oxide phase.

2. Distinct particles of some oxide phase with the main size of crystallites about 100 Å are detected; these particles might be attributed to (Zn-)Co oxide. The direct measurement of the lattice parameter of the Co oxide from HREM images indicates that it should be attributed to CoO. Oxidized state of Co might be the consequence of the exposure of the sample to air during its preparation for TEM study.
3. Few particles of Co_3O_4 of a "hollow speroidal shape", which is discussed below, are also present in the sample.

The TEM and HREM data on the sample P/ZS reduced at 800°C (Fig. 10) evidence that:

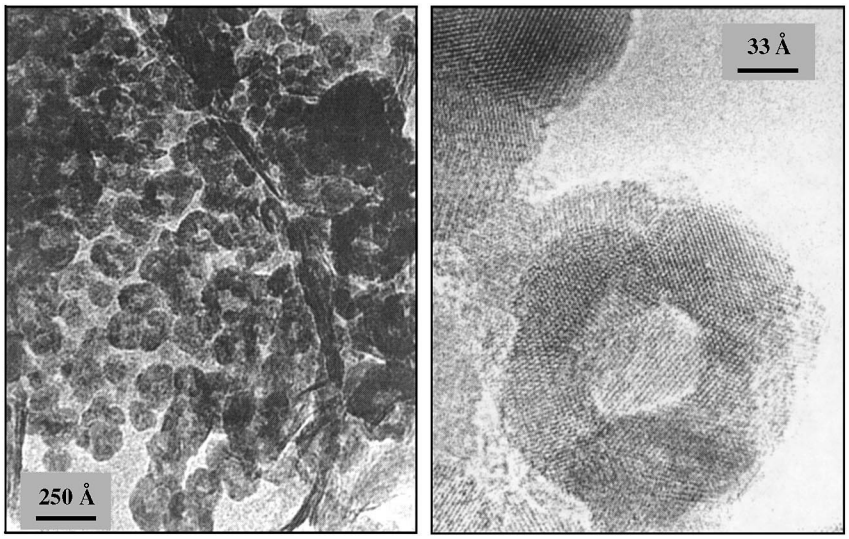

Fig. 11. TEM (left) and HREM (right) images of the sample P/ZS after its consecutive treatment in the inert gas flow at 450°C, then the H_2 flow at 450°C and the oxidation in air at 350°C.

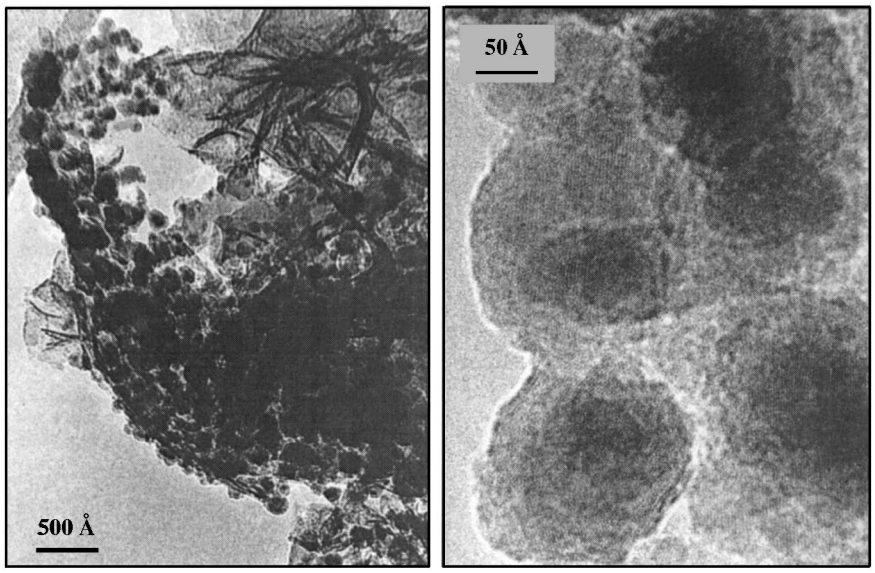

Fig. 12. TEM (left) and HREM (right) images of the sample P/ZS after its consecutive treatment in the inert gas flow at 450°C, then the H_2 flow at 450°C, the oxidation in air at 350°C and, finally, the re-reduction at 450°C.

1. SiO_2 plates and Co^0 are the only two phases, which are detectable.
2. Co^0 crystallites are globular particles with diameter from 100 to 800 Å, "attached" to the SiO_2 plates and covered with 20–50 Å film of SiO_2.
3. Few of the spatial defects are present in most of Co^0 particles.

XRD pattern of this sample contains the lines of β-Co^0 and α-Co^0, which may be attributed to the "defective interchange of coherent domains with fcc and hex structures" as it was described above. The size of the coherent reflectance domain estimated from $[1\,1\,1]_{fcc}$ line broadening is about 250 Å. No other well crystallized phase was detected by XRD in the sample. FTIR spectrum of the sample contain only the bands of SiO_2 (absorption at ca. 1100, 810, and 470 cm^{-1}). The results of TEM, XRD and FTIR are in good agreement with the results of the recent study on the evolution of Co–Zn-stevensites [11].

One can see from Fig. 11, that the Co_3O_4 particles of a "hollow spheroidal shape" (i.e. spehroids, hollow inside) are the main Co-containing phase, which comprise the sample P/ZS calcined at 450 in the Ar, reduced at 450°C, and oxidized in Air at 350°C. The hollow spheroids have the outer diameter of 150–300 Å and are composed by crystallites of 50–100 Å in diameter. They are similar to the particles observed earlier by Kepinsky and coauthors in [37] and described as the "torus shaped" ones. However, we suppose, that the particles have a spheroidal shape rather than torus, because we could not find a "raft"-shaped side projection of the torus in our TEM-patterns.

No "hollow spheroidal" particles can be detected in the sample P/ZS calcined at 450 in the Ar, reduced at 450°C, oxidized in Air at 350°C and re-reduced at 450°C (Fig. 12). The globular metallic Co particles, covered with Co oxide, are present. Their main size is 100–140 Å. The oxidized state of Co (a Co oxide film) seems to be a consequence of the exposure of the sample to air during its preparation for the TEM study. It is important to note, that HREM image of the re-reduced sample is much more distinct, than that for the sample P/ZS being reduced for the first time.

3.2. Catalytic tests

The data on the performance of the catalysts studied in the Fischer–Tropsch synthesis are present in Table 3. The CO conversion extent was maintained at

Table 3
Catalytic tests data

Sample	P/ZS	N/ZS	P/MS	A/MS	P/MgO
Co loading (wt.%)	21	21	27	27	60
Amount of Co^0 which is able to oxidize at $T < 350°C$, % of Co loading	32.4	42.7	32.5	54.0	61
Co^0 particle size (nm)	11[a,b]	14[b]	12[b]	12[b]	9[a,b]
Dispersion of Co^0[c]	0.09	0.08	0.10	0.10	0.12
Amount of surface Co^0 atom ($\mu mol\,g^{-1}$ cat.)	104	122	149	247	732
$T = 483\,K$					
CO conversion rate ($\mu mol\,g\,cat.\,h^{-1}$)	96	115	79	212	2573
CO conversion TOF (mol/Co at. s^{-1})	2.5×10^{-4}	2.6×10^{-4}	1.5×10^{-4}	2.4×10^{-4}	9.8×10^{-4}
CH_4 formation rate ($\mu mol\,g^{-1}\,cat.\,h^{-1}$)	14.8	28.1	29.9	78	198
CH_4 formation TOF (mol/Co at. s^{-1})	3.9×10^{-5}	6.4×10^{-5}	5.6×10^{-5}	8.8×10^{-5}	7.5×10^{-5}
ASF parameter α for saturated C_3–C_8	0.75	0.60	0.71	0.72	0.82[d]
ASF parameter α for olefins C_3–C_8	0.72	0.56	0.64	0.69	0.78[d]
Ratio of propene to propane	4	2	0.8	1.4	0.9
$T = 503\,K$					
CO conversion rate ($\mu mol\,g^{-1}\,cat.\,h^{-1}$)	160	206	110	344	3100
CO conversion TOF (mol/Co at. s^{-1})	4.3×10^{-4}	4.7×10^{-4}	2.1×10^{-4}	3.9×10^{-4}	12×10^{-4}
CH_4 formation rate ($\mu mol\,g^{-1}\,cat.\,h^{-1}$)	50	72	48	171	530
CH_4 formation TOF (mol/Co at. s^{-1})	13×10^{-5}	16×10^{-5}	8.9×10^{-5}	19×10^{-5}	20×10^{-5}
ASF parameter α for saturated C_3–C_8	0.70	0.54	0.58	0.71	0.82[d]
ASF parameter α for olefins C_3–C_8	0.58	0.49	0.56	0.65	0.78[d]
Ratio of propene to propane	6	2.3	1.2	3.5	0.9

[a] From TEM data.

[b] From XRD data on the $[1\,1\,1]_{fcc}$ peak broadening (the XRD pattern of a 'defective spacial-modulated interchange of coherent domains with fcc and hex structures').

[c] Ratio of the surface metal atoms amount to the total amount of metal atoms was estimated from the experimental value of the average particle diameter, d, considering the cuboctahedral shape of a particle, as it was made in [38].

[d] The same value of the ASF parameter α was obtained from evaluation of the experimental data on C_{15}–C_{24} hydrocarbons formation rate.

10–15% for all the catalytic test, which are discussed below. The activity of sample A/ZS was found to be lower, than our limits of adequate testing. Despite it was not absolutely inactive, we hesitate to trust the measured data. Catalyst P/MgO was tested as a reference catalyst, which can be supposed the one, which is free from a 'metal-support interaction'.

Co/ZS samples were calcined in the static air at 450°C, then reduced at 470°C and placed in *n*-tetradecane (slurry filling) without exposure to air. Co/MS samples were calcined in the inert gas flow at 450°C and reduced at 500°C.

One can see from the present data, that the studied samples exhibit an unexpectedly low activity in the CO hydrogenation. The rate of the CO conversion related to 1 g of a catalyst is 50 times less, than it was found for the P/MgO catalyst at the same CO conversion extent. The observed lack of activity cannot be explained by a low reduction extent of the Co/stevensite catalysts. The values of the turnover frequency of the CO conversion, TOF_{CO} (the specific activity in the CO conversion related to one surface Co^0 atom), which were estimated, considering only those Co^0 atoms, which can be 'easily' oxidized, are still three to six times lower than that for P/MgO catalyst. From another hand, the values of TOF_{CH_4} (turnover frequency of the methane formation) for the Co/stevensite catalysts are of the same value, that it is for P/MgO. This indicates, that the existing Co^0 species are nevertheless active in the reaction of the CO methanation. The discrepancy becomes smaller at higher temperature of the reaction (503 K). The measured values of α are significantly lower, than those expected to Co^0 which has the observed dispersion.

Earlier, Kuznetsov and coauthors [39,40] studied FTS on the ultradispersed Co/SiO_2 and Co/TiO_2, derived from dicobaltoctacarbonyl complex. It was shown by means of IRS of adsorbed CO, that the CO dissociation is slow over the surface of ultra-dispersed Co particles (10–20 Å). Simultaneously it was shown, that the activity of the CO conversion is 5–10 times lower over these catalysts in comparison with the 100 Å Co^0 crystallites. The value of α decreased significantly while decreasing the diameter of the Co^0 particles, i.e. when decreasing the rate of the CO dissociation.

Thus, one may suppose that a slow CO dissociation over the Co/ZS and Co/MS catalysts is the reason of the observed performance of these catalysts in the Fischer–Tropsch synthesis. However, the TEM and XRD data evidence, that the main size of the Co^0 species is at least above 10 nm. In this range of the Co^0 particle size, the dispersion was shown not to affect the turnover frequency of the CO conversion over a Co^0 surface atom (see [5,41]).

3.3. The plausible nature of the active component of Co/stevensite

The possible reason for the observed phenomenon is an effect of the support on the nature and catalytic properties of the active component. It is well known, that Ni supported by Rutile TiO_2 differs sufficiently from Ni^0 supported by Al_2O_3 or SiO_2 by its catalytic properties due to 'strong metal-support interaction' (SMSI) (see review [42]). The CO adsorption over Ni^0/TiO_2 surface is much less, than it can be expected from the experimental data on the Ni^0 particle size, which is related to the formation of the TiO_x species on the active component surface. From another hand, the specific activity of Ni^0/TiO_2 in the CO hydrogenation is manifold greater, than it was determined for the Ni/MgO or Ni^0 foil. In addition, the selectivity of Ni in the 'SMSI state' is shifted to the formation of higher hydrocarbons. This is related usually to an effect of a negative charging of the Ni^0 species at the expense of the TiO_2 support, which was found to hold plenty of oxygen vacancies at the surface. The presence of excess electrons in the active component particles increases their electron-donor ability and makes the dissociation of CO to be more easy due to settling of the antibonding orbitals of CO.

One can note, that the 'SMSI' effect is quite opposite to what we observe for Co/stevensite catalysts. At that, 'SMSI' effect was not observed for SiO_2-supported catalysts. In [5], Co-containing catalysts prepared by impregnation with $Co(NO_3)_2$ were found to be insensitive to the support nature (among SiO_2, Al_2O_3 and TiO_2). This study was performed using the catalysts prepared by impregnation of the support with concentrated Co nitrate, thus no interaction of silica with Co species can be expected.

Co-containing catalysts supported by "silicate crystallite mesoporous material or SCMM", which was prepared from Si, Mg and Al in the hydrothermal conditions along with the quaternary ammonium salt, were studied in [43]. The structure of the SCMM support is close to the smectite (Al^{3+}-substituted stevensite) structure. The catalytic properties of these catalysts were found to be sensitive to the distribution of the charge within the support crystallite. The important feature of these catalysts was found the existence of linear CO species absorbed on Co^0 particles.

In [44], the Co-pillared clays (incl. Co-pillared stevensite) were studied in reactions of hydrodesulfurization. The authors of [44] had concluded that Co^+ species are forming during the reduction of the Co-pillared clay at 450°C. The formation of these species was related to the peculiarity of the clay structure, which is able to keep the cation vacancy, after the Co^{2+} cation was reduced. Transferring the conclusion of [44] onto the samples under our study, one may suppose that a partial reduction of few Co^{2+} cations from the Co–Me-stevensite support can occur at 450°C, resulting in the formation of cationic vacancies and to positive charging of the Co^0 particles. However, this hypothesis needs thorough examination by both kinetic and physical methods.

4. Conclusions

The cobalt catalysts supported over synthetic stevensites of Zn and Mg were prepared by few different methods. It was shown that a significant amount of Co^{2+} (at least 17%) is included in the stevensite structure, substituting Zn and Mg at the stage of the catalyst calcination. The catalysts prepared by impregnation with acetates are more liable to such interaction of Co^{2+} with the support.

The amount of Co^{2+} located in the octahedral stevensite sites increases after the reduction–oxidation procedure and achieves 50%. The Co^{2+} cations substitute Mg^{2+} more easily, than the Zn^{2+} cations.

The catalysts in their reduced state contain a Co^0 phase, which is highly defective and contains an interchange of coherent domains with fcc and hex structures. This was proved by the TEM and XRD data.

The catalytic performance of the studied catalysts in the FTS is rather poor and is characterized by low TOF of the CO conversion and low values of the ASF parameter α. A positive point of these catalysts is their high olefins-to-paraffins ratio.

We attribute the observed catalytic performance to the effect of the stevensite support on the state of the active component. The observed catalytic performance might be explained by a slow CO dissociation over the Co^0/stevensite, caused by a low electron-donor capacity of the metallic particles.

Acknowledgements

This research work was implemented by the finance by PEC, Japan.

References

[1] D.G. Castner, P.R. Watson, I.Y. Chan, J. Phys. Chem. 93 (1989) 3188.
[2] A. Lapidus, A. Krylova, V. Kazanskii, V. Borovikov, A. Zaitsev, J. Rathousky, A. Zukai, M. Jancalkowa, Appl. Catal. 73 (1991) 65.
[3] Y. Okamoto, K. Nagata, T. Adachi, T. Imanaka, K. Inamura, T. Takyu, J. Phys. Chem. 95 (1991) 310.
[4] H. Ming, B.G. Baker, Appl. Catal. A: Gen. 123 (1995) 23.
[5] E. Iglesia, Appl. Catal. A: Gen. 161 (1997) 59.
[6] E. Iglesia, S.L. Soled, J.E. Baumgartner, S.C. Reyes, J. Catal. 153 (1995) 108.
[7] I. Puskas, T.H. Fleisch, J.B. Hall, B.L. Meyers, R.T. Roginsky, J. Catal. 134 (1992) 615.
[8] L.B. Backman, A. Rautiainen, A.O.I. Krause, M. Lindblad, Catal. Today 43 (1998) 11.
[9] E. van Steen, G.S. Sewell, R.A. Makhothe, C. Micklethwaite, H. Manstein, M. de Lange, C.T. O'Connor, J. Catal. 162 (1996) 220.
[10] A. Barbier, A. Hanif, J.A. Dalmon, G.A. Martin, Appl. Catal. A: Gen. 168 (1998) 333.
[11] A.A. Khassin, T.M. Yurieva, G.N. Kustova, L.M. Plyasova, T.A. Krieger, I.Sh. Itenberg, M.P. Demeshkina, V.F. Anufrienko, T. Larina, V.N. Parmon, Mater. Res. Innov. 4 (2000), in press.
[12] A.A. Khassin, T.M. Yurieva, L.M. Plyasova, V.I. Zaikovskii, V.N. Parmon, unpublished results.
[13] G.J. Haddad, B. Chen, J.G. Goodwin Jr., J. Catal. 161 (1996) 274.
[14] B. Ernst, A. Bensaddik, L. Hilaire, P. Chaumette, A. Kiennemann, Catal. Today 39 (1998) 329.
[15] M. Adachi, K. Yoshii, Y.Z. Han, K. Fujimoto, Bull. Chem. Soc. Jpn. 69 (1996) 1509.
[16] A. Feller, M. Claeys, E. van Steen, J. Catal. 185 (1999) 120.
[17] B. Ernst, S. Libs, P. Chaumette, A. Kiennemann, Appl. Catal. A: Gen. 186 (1999) 145.
[18] T.M. Yurieva, G.N. Kustova, T.P. Minyukova, E.K. Poels, A. Bliek, M.P. Demeshkina, L.M. Plyasova, T.A. Krieger, Mater. Res. Innov. 4 (2000), submitted for publication.
[19] C.J.G. van der Grift, P.A. Elberse, A. Mulder, J.W. Geus, Appl. Catal. 59 (1990) 275.
[20] D.A.M. Monti, A. Baiker, J. Catal. 83 (1983) 323.
[21] B. Ernst, S. Libs, P. Chaumette, A. Kiennemann, Appl. Catal. A: Gen. 186 (1999) 145.
[22] T.A. Krieger, L.M. Plyasova, T.M. Yurieva, Mater. Sci. Forum 321–324 (Part 1) (1999) 386.
[23] P.A. Ramachandran, R.V. Chaudhari, Three-Phase Catalytic Reactors, Gordon and Breach, New York, 1983.
[24] K. Nakamoto, Infrared and Raman Spectra of Inorganic and Coordination Compounds, Wiley, New York, 1986.
[25] A.A. Khasin, T.M. Yureva, V.I. Zaikovskii, L.M. Plyasova, V.N. Parmon, Kinet. Catal. Engl. Tr. 39 (3) (1998) 400 (The official English translation from Kinet. Catal. 39 (3) (1998) 431).
[26] G.G. Volkova, T.M. Yurieva, G.N. Kustova, L.M. Plyasova, G.V. Kharlamov, G.S. Litvak, V.F. Anufrienko, Zhurn. Prikl. Khimii 67 (4) (1994) 779 (in Russian).
[27] A.A. Khassin, Ph.D. Thesis, Boreskov Institute of Catalysis, Novosibirsk, 1998 (in Russian).
[28] PCPDF Win, Ver 1.30, JCPDS ICDD, Swarthmore, PA, USA, 1997, pp. 36–451.
[29] A.B.P. Lever, Inorganic Electron Spectroscopy, Studies in Physical and Theoretical Chemistry, 33, Vol. 2, Elsevier, Amsterdam, 1984.
[30] R. Pappalardo, D.J. Wood, R.C. Linares Jr., J. Chem. Phys. 35 (1961) 2041.
[31] N.G. Maksimov, L.I. Kuznetsova, V.F. Anufrienko, T.M. Yurieva, Izv. SO AN SSSR Inorg. Mater. Ser. 12 (7) (1976) 1219.
[32] PCPDF Win, Ver 1.30, JCPDS ICDD, Swarthmore, PA, USA, 1997, pp. 15–806.
[33] PCPDF Win, Ver 1.30, JCPDS ICDD, Swarthmore, PA, USA, 1997, pp. 5–727.
[34] S.V. Tsybulya, S.V. Cherepanova, A.A. Khassin, V.I. Zaikovskii, V.N. Parmon, Doklady Phys. Chem. 366 (1–3) (1999) (The official English translation from Doklady RAN 366 (2) (1999) 216).
[35] A.J.C. Wilson, X-Ray Optics, Methuen, London, 1949.
[36] A. Guinier, Theorie et Technique de la Radiocristallographie, DUNOD, Paris, 1956.
[37] D. Potoczna-Petru, J.M. Jablonski, J. Okal, L. Kepinski, Appl. Catal. 175 (1998) 113.

[38] A. Barbier, E.B. Pereira, G.A. Martin, Catal. Lett. 45 (1997) 221.
[39] A.S. Lisitsyn, A.V. Golovin, V.L. Kuznetsov, Yu.I. Yermakov, J. Catal. 95 (1985) 527.
[40] V.L. Kuznetsov, M.N. Aleksandrov, L.N. Bulgakova, J. Mol. Catal. 55 (1989) 146.
[41] S.W. Ho, M. Houalla, D.M. Hercules, J. Phys. Chem. 94 (1990) 6396.
[42] J.P.S. Badyal, in: D.A. King, D.P. Woodruff (Eds.), The Chemical Physics of Solid Surfaces, Vol. 6, Elsevier, Amsterdam, 1993, Chapter 10, p. 311.
[43] T. Iwasaki, M. Reinikainen, Y. Onodera, H. Hayashi, T. Ebina, T. Nagase, K. Torii, K. Kataja, A. Chatterjee, Appl. Surf. Sci. 130–132 (1998) 845.
[44] E. Hayashi, E. Iwamatsu, M.E. Bismas, Y. Sanada, S. Ahmed, H. Hamid, T. Yoneda, Appl. Catal. A: Gen. 179 (1999) 203.